Amplification of pyroelectric device with WSe2 field effect transistor and ferroelectric gating

Amplification of Pyroelectric Device with WSe_2 Field Effect Transistor and Ferroelectric Gating

Stephen C. Mbisike[1,a)], Lutz Eckart[2], John W. Phair[2], Peter Lomax[1] and Rebecca Cheung[1]

AFFILIATIONS

[1] Scottish Microelectronics Centre, Institute for Integrated Micro and Nano Systems, School of Engineering, University of Edinburgh, EH9 3FF, U.K

[2] Pyreos Limited, Kings Buildings, Edinburgh, U.K

[a)] Corresponding author's email: stephen.mbisike@ed.ac.uk

ABSTRACT

A WSe_2 Field Effect Transistor (FET) integrated with a Lead Zirconium Titanate (PZT) pyroelectric device has been designed, fabricated, tested and is described as the integrated pyroelectric device (IPD). The integrated device has been compared to a standalone pyroelectric device (SPD) which consists of PZT sandwiched between platinum electrodes. A pyroelectric coefficient of $1.755*10^{-4}$ C/m^{2}K has been realized for our thin-film PZT (650 nm). The integrated device amplifies the output of the standalone device by over ten orders of magnitude as the current density calculated for the devices is 16 nA/mm^2 and 1 nA/mm^2 respectively. The interplay between the pyro and ferro-induced polarization of the integrated device has been studied. From our observations, the ferroelectric gating controls directly the drain-source current output of the integrated device, showing anti-clockwise hysteresis behaviour. The device shows promise for application in infrared sensing.

***Index Terms*—**WSe_2, PZT, field effect transistor (FET), standalone pyroelectric device (SPD), integrated pyroelectric device (IPD).

I. Introduction

Since the discovery of infrared (IR) about two centuries ago[1], IR detectors have found applications in medical imaging, military equipment, environmental sensing amongst others[2]. Pyroelectric devices are employed in IR detectors and are finding increased application in IR sensing[2], [3]. Pyroelectricity is the property of certain crystals to spontaneously polarize in response to a change in temperature [4]. Thin film pyroelectric IR detectors have been produced from Lead Zirconium Titanate (PZT) and the pyroelectric current measured as a result of changes in temperature. The current so measured is dependent on device area and typically in the order of tens of pico-amps [5]. Graphene and 2-dimentional (2D) transition metal dichalcogenides (TMD) have been integrated with a pyroelectric device to improve the output signal of the IR detector [2] and performance of the 2D FET [6] respectively.

TMDs such as tungsten diselenide (WSe_2) and molybdenum disulfide (MoS_2) have found increased applications in electronic devices by virtue of their promising electronic band structure [7]. TMDs consists of one atom of a transition metal and two atoms of a chalcogen element covalently bonded together (X-M-X). The atoms form hexagonal arrangement and adjacent planes are held together by weak van der waals interaction [8]. As a result of this weak bonding, layers of TMDs can be exfoliated and deposited onto a substrate for further processing. PZT is increasingly employed for ferroelectric field effect transistor devices owing to its high capacitance, low coercive field, chemical stability and compatibility with fabrication processes.

In this work, standalone pyroelectric device (SPD) made from PZT with a top and bottom electrode has been fabricated and the pyroelectric current measured with respect to temperature. Also, 45 nm thick WSe_2 has been exfoliated and deposited onto the thin film PZT. WSe_2 FET has been integrated with PZT (IPD) with a view to amplify the device output. The characteristics of the SPD and the IPD as a function of temperature have been analyzed. In addition, the PZT based WSe_2 FET has been gated and the transfer characteristics of the device has been studied.

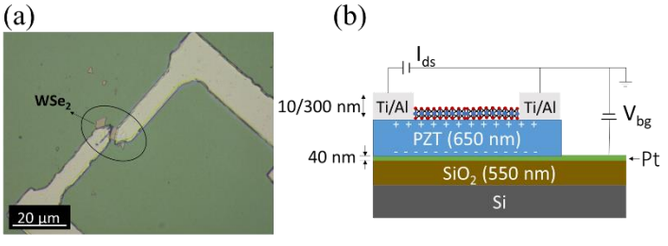

Fig. 1. (a) Device fabricated showing WSe_2 FET with metal electrodes on PZT (IPD). (b) Schematic of WSe_2-PZT FET on a SiO_2/Si substrate.

II. Device Design, Fabrication and Characterization

The devices have been fabricated using microfabrication processes. The PZT has been sputtered from individual target of the constitute elements at about 600 °C forming thin-film

PZT. Both the platinum and PZT have been deposited via sputtering onto the SiO_2 substrate. Using scotch-tape, the WSe_2 flake has been exfoliated and deposited onto the PZT substrate. By mask-less lithography, the photoresist has been patterned and the metal electrodes (Titanium/Aluminum) deposited as the source and drain. Figure 1a shows the 45 nm thick WSe_2 flake on PZT with the metal electrodes. Atomic force microscopy has been used to confirm the thickness of the WSe_2 flake. Figure 1b shows the device schematic entailing the material stack and electrical connections. The platinum serves as the bottom electrode for gating the device. The devices have been tested using a Keithley parameter analyzer fitted with a temperature chuck. The temperature chuck is connected to the ATT-Systems module responsible for controlling and measuring the temperature. Temperature values of between 21- 32 °C have been applied to the measurements. Additionally, scanning electron microscopy (SEM) and electron back scatter diffraction (EBSD) have been performed on the PZT to study its crystal quality. The SEM and EBSD experiments have been carried out using a Carl Zeiss SIGMA HD VP field emission SEM with Oxford Instruments Aztec Synergy EBSD system. For SEM, an accelerating voltage of 3 kV and a working distance of approximately 5.5 mm has been applied. The EBSD conditions entails a 70 degrees tilt of the sample, 10 kV accelerating voltage and working distance of ~12.5 mm.

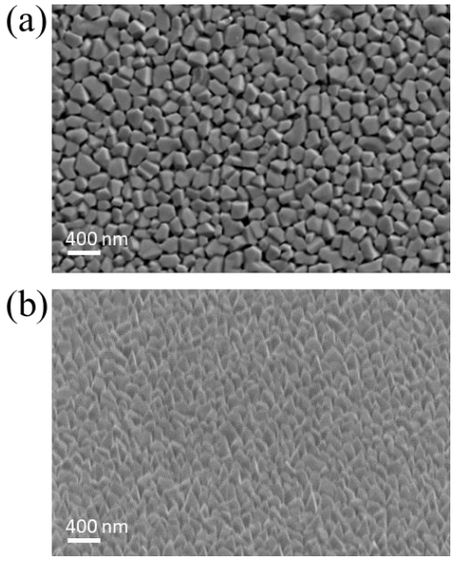

Fig 2: (a) PZT crystals on high magnification SEM (b) PZT crystals tilted at 70° for EBSD

The images in Fig 2 are standard secondary electron (SE) images of the surface of the PZT. The SEM image in Fig 2a has been taken directly from the top of the sample and the grain size is about 100 nm. However, the image in Fig 2b has been taken from a 70° tilt and it can be seen that many of the crystals grow to the pyramid shape. Some of the crystals being pointed at the top and some narrowing, but not quite forming a point.

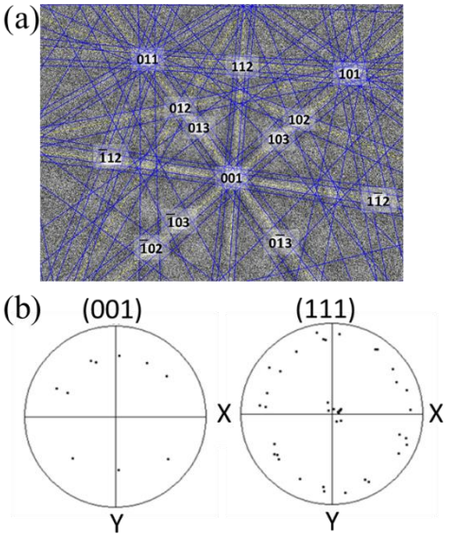

Fig 3: (a) Electron diffraction pattern of a single point on the PZT (b) Pole figures of the (001) and (111) crystal facet, mapped from a single PZT grain

Fig 3a shows the diffraction pattern formed by the electron beam interacting with a single point on the 70° tilted PZT sample grown on platinum (Pt) bottom electrode. With the aid of the Aztec system database, a solution for the diffraction pattern has been indexed (Tetragonal, Space Group 99) [9]. The successful detection of the electron diffraction pattern and the consequent indexing (Fig. 3(a)) indicates that the PZT exists in tetragonal crystals. In addition, an area of single crystal grains from the PZT has been mapped, and plotted in the pole figure (Fig. 3(b)) with the assistance of the MTEX program. It can be seen that for the PZT, the data points of the (111) crystal facet are gathered in the centre and side of the pole figures, and the data points of the (100) crystal facet are gathered on the side, indicating a tetragonal shape. The pole figures indicate that PZT grown on Pt seed layers show good correlation for an orientation along the [111] direction normal to the sample surface in agreement with [10].

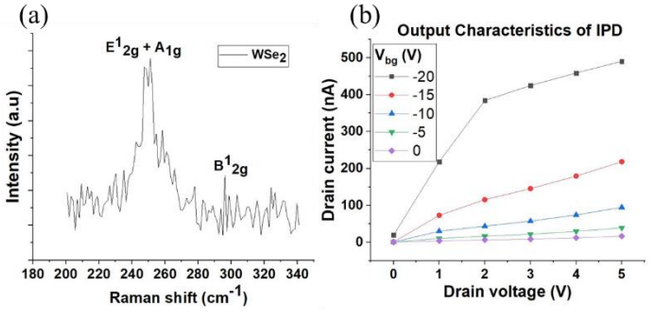

Fig 4. (a) Raman shift of the 45 nm thick WSe_2 flake (b) Output characteristics of WSe_2-PZT FET with gate voltage running from 0 to -20 V.

To characterize the quality of the WSe_2, Raman spectroscopy has been performed on the 45 nm thick WSe_2 shown in Fig 4(a). In-plane E^1_{2g} mode from the out-of-phase vibration and

A_{1g} mode from the out-of-plane vibrations of WSe_2 both appear as a single peak (E^1_{2g} + A_{1g}) at 252 cm^{-1}. The Raman shift of about 252 cm^{-1} shows the WSe_2 is of good quality. The sample has been excited with a 450 nm laser under room temperature and atmospheric pressure. The B^1_{2g} indicates the sample is of several layers thick. The B^1_{2g} peak intensity diminishes as the number of layers increases in response to vibrational dampening coming from lower interlayer interaction [11].

Fig 4(b) shows the output characteristics of the IPD gated from 0 to -20 V with a step gate voltage of 5 V and a sweeping drain-source voltage (V_{ds}) from 0 to 5 V. The plots begin linearly and as V_{ds} increases, the drain-source current (I_{ds}) begins to pinch-off as it nears saturation indicating generic MOSFET behaviour.

III. RESULTS AND DISCUSSION

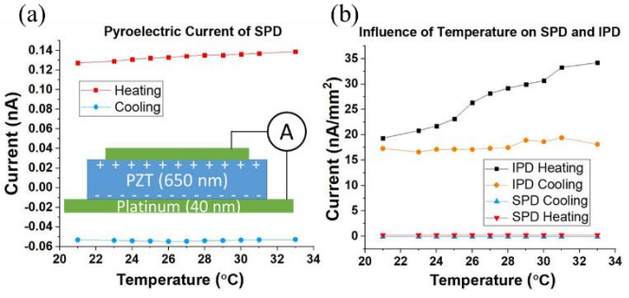

Fig 5. (a) Pyroelectric current of the SPD against temperature. The inset figure shows the schematic of the SPD. (b) Comparison of the current density of the IPD and SPD under the influence of temperature change only.

The schematic in the inset of Fig 5 (a) shows the PZT sandwiched with a top and bottom metal electrode. The device dimensions allow for the detection of infrared radiation [12]. Due to the thickness of the PZT, infrared wavelength can be converted into heat resulting in the release of charge from the pyroelectric effect. Pyroelectric materials do not rely on the *Seebeck* effect [13], and can be deployed in a spatially uniform temperature environment. The device has been tested against changes in temperature both during heating and cooling. From Fig 5(a), the pyroelectric current measured during heating (21 – 32 °C) of the device stands around 124 – 145 pA whilst about 46 – 55 pA was measured during cooling (32 – 21 °C). The higher pyroelectric current magnitude observed during heating is attributed to a higher degree of polarization in the PZT during heating. The degree of polarization in this instance is a factor of the rate of change of temperature of the heating element which heats up faster than it cools. Additionally, piezoelectric effect could arise from material expansion and this is believed to be responsible for the unstable pyroelectric current measured during heating. The change in polarity of the measured pyroelectric current is a result of the reversal in polarization of the pyroelectric device and consequently, its dipole moment [14]. The area of the SPD top electrode is 0.64 mm^2 and the pyroelectric coefficient of the PZT has been calculated to be $1.755*10^{-4}$ C/m^2K using eq 1.

$$p = \frac{i}{A * (dT/dt)} \qquad (1)$$

Where: p = Pyroelectric coefficient; i = pyroelectric current; A = Area; dT/dt = rate of change in temperature.

Similar PZT based pyroelectric device has been demonstrated by [5] and has been tested across a temperature range of 30 – 60 °C, producing a current output of about 100 to 120 pA. Yang et al. reported on a PZT nanogenerator that is 175 mm thick and 5 mm in electrode length which produces a pyroelectric current of about 430 nA [15].

The effect of temperature change on the output current of both the IPD and the SPD is shown in Fig 5(b). The SPD plots in red and blue depict the pyroelectric current density of 1 – 1.8 nA/mm^2 and 0.8 – 1 nA/mm^2 for heating and cooling respectively. On the other hand, the IPD represented by the black and orange plots has been biased with a V_{ds} of 1 V. The current density measured during heating is about 20 – 35 nA/mm^2 whilst 16 – 19 nA/mm^2 has been measured during cooling. The combined area of the WSe_2 and the electrodes is about 0.0526 mm^2. No gate voltage has been applied and the IPD shows an amplified current output of over ten (10) order of magnitude higher than what is obtainable from the SPD. It is believed that a combined bolometric and pyroelectric effect is responsible for the measured output of the IPD. It is possible that absorbed heat could affect the temperature coefficient of resistance (TCR) of the WSe_2, ultimately affecting the current output of the device. Additionally, the temperature change can result in the release of charges due to the pyroelectric effect which in turn modulates the WSe_2 resistance [2].

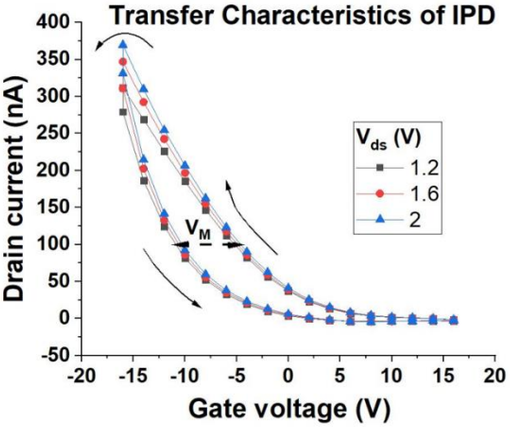

Fig 6. Transfer characteristics of WSe_2-PZT FET (IPD) showing ferroelectric behaviour. Gate voltage is applied from -16 V to 16V with a step of 2 V.

To investigate the ferroelectric behaviour of the IPD, the device has been back-gated from -16 to 16 V under varied drain-source voltage (V_{ds}). In Fig 6, each loop represents the ferroelectric response of the WSe_2 FET to the polarization of the PZT. The point where the drain-source current (I_{ds}) is maximum represents the maximum polarization achieved by

the PZT. It can be seen that the maximum I_{ds} is 0.36 µA when the maximum gate voltage (V_{gs}) is -16 V. Similar current output of 0.5 µA has been realized from a ferroelectric FET based on WSe_2 on $CuInP_2S_6$ [16]. The hysteresis direction of the IPD is shown by the arrows in the graph, which is in the same direction as the polarization versus voltage (P-V) curve [17]. Hence, the IPD shows good ferroelectric response as it has the expected anti-clockwise hysteresis behavior in sync with the polarization effects of the ferroelectric gate dielectric. Similar anti-clockwise hysteresis graphs have been obtained for MoS_2 FET [18]. The actual origin of hysteresis is still under debate, however, the postulated reasons for current–voltage hysteresis include: the ferroelectric effect, ionic motions within the ferroelectric material and charge trapping and detrapping [19], [20]. The ferroelectric effect can be described as spontaneous electric polarization induced in dielectrics by an applied electric field [21]. Research has shown that ferroelectric crystals can change symmetry which in turn, can affect charge carrier extraction [22]. Ionic migration occurs in ferroelectrics under a voltage bias and leads to a build-up of internal potential. The speed of the ion migration can have an effect on the current-voltage hysteresis. Furthermore, charge traps formed as a result of defects within the ferroelectric material can further explain the origin of hysteresis[19], [20]. These trapped electrons and holes significantly affect the charge transport properties of the material [23]. Additionally, V_M in Fig 6, represents the memory window and is defined as the difference in V_{gs} that occurs at the current value corresponding to the midpoint of the maximum and minimum possible current values of the device. As can be seen in the figure, the V_M of each loop is similar in range despite changes in the V_{ds} from 1.2 to 2 V, indicating the stability of the memory window. The memory window for this device is about 7 ± 1 V for a V_{gs} range of 32 V (-16 to 16 V). The memory window in this experiment is comparable to the memory window of MoS_2-PZT FET indicating possibility for memory application [24].

The data from Fig 5b and Fig 6 show the effects of temperature and electric field on the IPD respectively. From changes in the IPD temperature (21 – 32°C) in Fig 5b, a corresponding increase in output current density of about 15 nA/mm^2 has been observed. In comparison to the effect of gate voltage (0 to -15V) in Fig 6, a corresponding current output of about 370 nA (7 µA/mm^2) has been observed. It could be concluded that higher polarization in PZT is realized from the gate voltage via the ferroelectric effect than from temperature change.

IV. CONCLUSION

The design, fabrication and operation of a WSe_2-PZT FET (IPD) and a PZT sandwiched between metal electrodes (SPD) has been presented. The current density output of the IPD and SPD is ~16 nA/mm^2 and ~1 nA/mm^2 respectively. Thus, the integrated device amplifies the current output of the standalone device by over ten orders of magnitude. In addition, it has been observed that the gate voltage induces more polarization in the PZT than temperature change alone. Anti-clockwise hysteresis behavior measured in the device shows direct control of PZT polarization on the WSe_2 FET. The performance of the PZT based WSe_2 FET would help guide future experiments to develop high performing electronic devices.

V. ACKNOWLEDGMENT

The work of S.C. Mbisike has been supported by the Petroleum Technology Development Fund (PTDF) and also by Pyreos Limited. S.C. Mbisike wishes to acknowledge Imo State University.
The authors would like to acknowledge the UK Engineering and Physical Sciences Research Council (EPSRC).

REFERENCES

[1] A. Rogalski, "Infrared detectors: an overview," *Infrared Physics & Technology*, vol. 43, no. 3, pp. 187–210, Jun. 2002, doi: 10.1016/S1350-4495(02)00140-8.

[2] U. Sassi *et al.*, "Graphene-based mid-infrared room-temperature pyroelectric bolometers with ultrahigh temperature coefficient of resistance," *Nature Communications*, vol. 8, p. 14311, Jan. 2017, doi: 10.1038/ncomms14311.

[3] H. Fang *et al.*, "Infrared light gated MoS_2 field effect transistor," *Opt. Express, OE*, vol. 23, no. 25, pp. 31908–31914, Dec. 2015, doi: 10.1364/OE.23.031908.

[4] J. C. Burfoot and G. W. Taylor, *Polar Dielectrics and their Applications*. London: Macmillan, 1979.

[5] R. Bruchhaus, D. Pitzer, R. Primig, M. Schreiter, and W. Wersing, "Sputtering of PZT thin films for surface micromachined IR-detector arrays," *Integrated Ferroelectrics*, vol. 25, no. 1–4, pp. 1–11, Sep. 1999, doi: 10.1080/10584589908210154.

[6] C. Zhou *et al.*, "Low voltage and high ON/OFF ratio field-effect transistors based on CVD MoS2 and ultra high-k gate dielectric PZT," *Nanoscale*, vol. 7, no. 19, pp. 8695–8700, May 2015, doi: 10.1039/C5NR01072A.

[7] J. A. Wilson and A. D. Yoffe, "The transition metal dichalcogenides discussion and interpretation of the observed optical, electrical and structural properties," *Advances in Physics*, vol. 18, no. 73, pp. 193–335, May 1969, doi: 10.1080/00018736900101307.

[8] R. Addou and R. M. Wallace, "Surface Analysis of WSe2 Crystals: Spatial and Electronic Variability," *ACS Appl. Mater. Interfaces*, vol. 8, no. 39, pp. 26400–26406, Oct. 2016, doi: 10.1021/acsami.6b08847.

[9] J. Joseph, T. M. Vimala, V. Sivasubramanian, and V. R. K. Murthy, "Structural investigations on Pb(ZrxT1−x)O3 solid solutions using the X-ray Rietveld method," *Journal of Materials Science*, vol. 35, no. 6, pp. 1571–1575, Mar. 2000, doi: 10.1023/A:1004778223721.

[10] R. Köhler, N. Neumann, N. Heß, R. Bruchhaus, W. Wersing, and M. Simon, "Pyroelectric devices based on sputtered PZT thin films," *Ferroelectrics*, vol. 201, no. 1, Art. no. 1, Sep. 1997, doi: 10.1080/00150199708228356.

[11] S. C. Mbisike, S. Seo, S. Lee, J. Phair, and R. Cheung, "Parametric study of pulsed laser deposited (PLD) WSe2 2D transistors," *Microelectronic Engineering*,

vol. 230, p. 111368, Jun. 2020, doi: 10.1016/j.mee.2020.111368.

[12] W. W. Salisbury, "Absorbent body for electromagnetic waves." U.S. Patent 2 599 944, Jun. 10, 1952.

[13] Y. Yang *et al.*, "Pyroelectric Nanogenerators for Harvesting Thermoelectric Energy," *Nano Lett.*, vol. 12, no. 6, pp. 2833–2838, Jun. 2012, doi: 10.1021/nl3003039.

[14] S. Lang, "The history of pyroelectricity: From ancient greece to space missions," 1999, doi: 10.1080/00150199908214903.

[15] Y. Yang, S. Wang, Y. Zhang, and Z. L. Wang, "Pyroelectric Nanogenerators for Driving Wireless Sensors," *Nano Lett.*, vol. 12, no. 12, pp. 6408–6413, Dec. 2012, doi: 10.1021/nl303755m.

[16] X. Jiang *et al.*, "Ferroelectric Field-Effect Transistors Based on WSe2/CuInP2S6 Heterostructures for Memory Applications," *ACS Appl. Electron. Mater.*, vol. 3, no. 11, pp. 4711–4717, Nov. 2021, doi: 10.1021/acsaelm.1c00492.

[17] R. Köhler, N. Neumann, N. Heß, R. Bruchhaus, W. Wersing, and M. Simon, "Pyroelectric devices based on sputtered PZT thin films," *Ferroelectrics*, vol. 201, no. 1, pp. 83–92, Sep. 1997, doi: 10.1080/00150199708228356.

[18] Z. Lu *et al.*, "Nonvolatile MoS2 field effect transistors directly gated by single crystalline epitaxial ferroelectric," *Appl. Phys. Lett.*, vol. 111, no. 2, p. 023104, Jul. 2017, doi: 10.1063/1.4992113.

[19] R. Singh and M. Parashar, "Origin of Hysteresis in Perovskite Solar Cells," in *Soft-Matter Thin Film Solar Cells*, AIP Publishing LLC, 2020, pp. 1-1-1–42. doi: 10.1063/9780735422414_001.

[20] D. H. Song *et al.*, "A discussion on the origin and solutions of hysteresis in perovskite hybrid solar cells," *J. Phys. D: Appl. Phys.*, vol. 49, no. 47, p. 473001, Nov. 2016, doi: 10.1088/0022-3727/49/47/473001.

[21] Y. Xu, *Ferroelectric Materials and Their Applications*. Amsterdam: Elsevier Science & Technology, 1991.

[22] C. Quarti, E. Mosconi, and F. De Angelis, "Interplay of Orientational Order and Electronic Structure in Methylammonium Lead Iodide: Implications for Solar Cell Operation," *Chem. Mater.*, vol. 26, no. 22, pp. 6557–6569, Nov. 2014, doi: 10.1021/cm5032046.

[23] Y. Wang *et al.*, "Trap-limited charge recombination in intrinsic perovskite film and meso-superstructured perovskite solar cells and the passivation effect of the hole-transport material on trap states," *Phys. Chem. Chem. Phys.*, vol. 17, no. 44, pp. 29501–29506, Nov. 2015, doi: 10.1039/C5CP04360C.

[24] X.-W. Zhang *et al.*, "MoS2 Field-Effect Transistors With Lead Zirconate-Titanate Ferroelectric Gating," *IEEE Electron Device Letters*, vol. 36, no. 8, pp. 784–786, Aug. 2015, doi: 10.1109/LED.2015.2440249.

AIP Publishing

Journal of Applied Physics

ACCEPTED MANUSCRIPT

PLEASE CITE THIS ARTICLE AS DOI: 10.1063/5.0086216

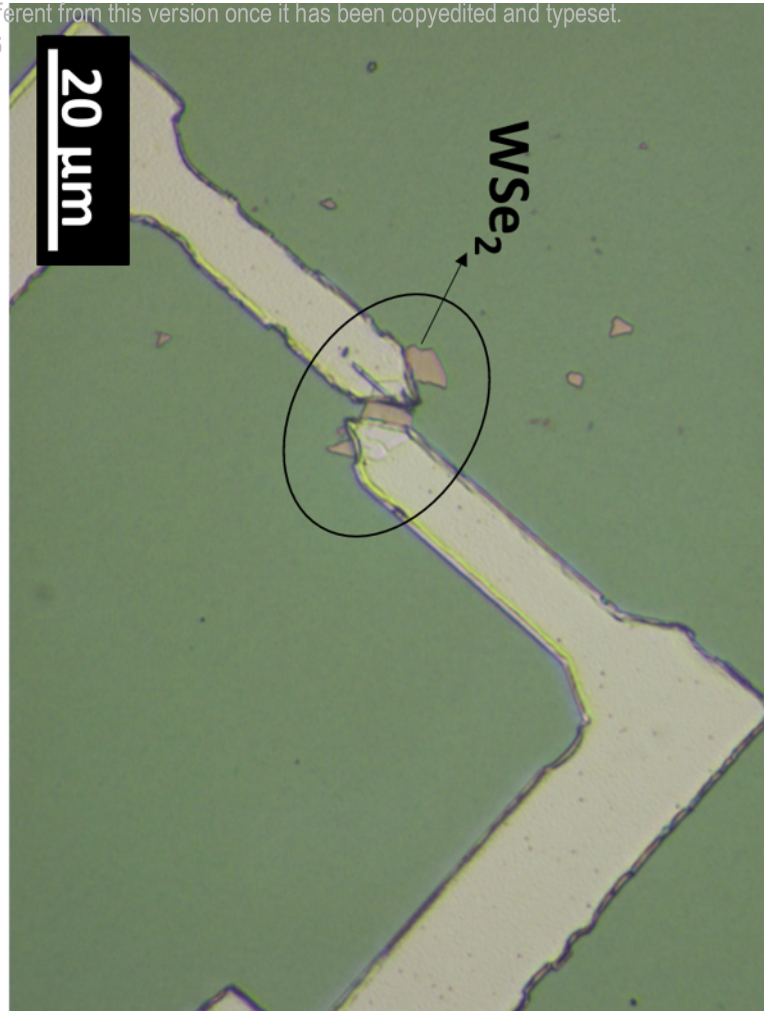

AIP Publishing

Journal of Applied Physics

ACCEPTED MANUSCRIPT

PLEASE CITE THIS ARTICLE AS DOI: 10.1063/5.0086216

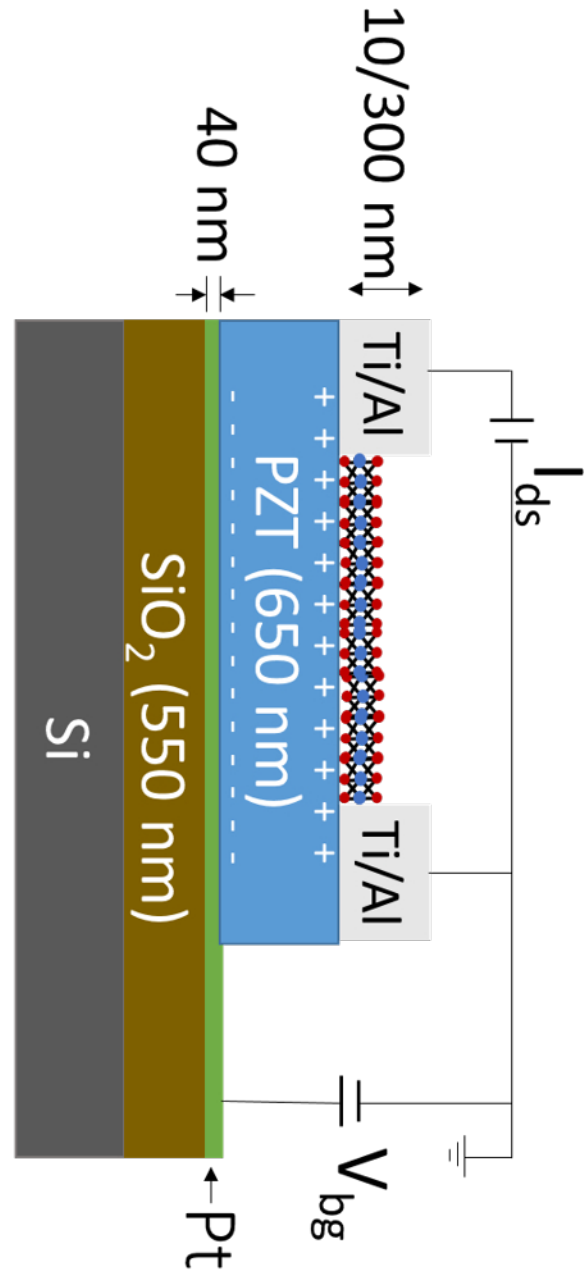

AIP Publishing

Journal of Applied Physics

ACCEPTED MANUSCRIPT

PLEASE CITE THIS ARTICLE AS DOI: 10.1063/5.0086216

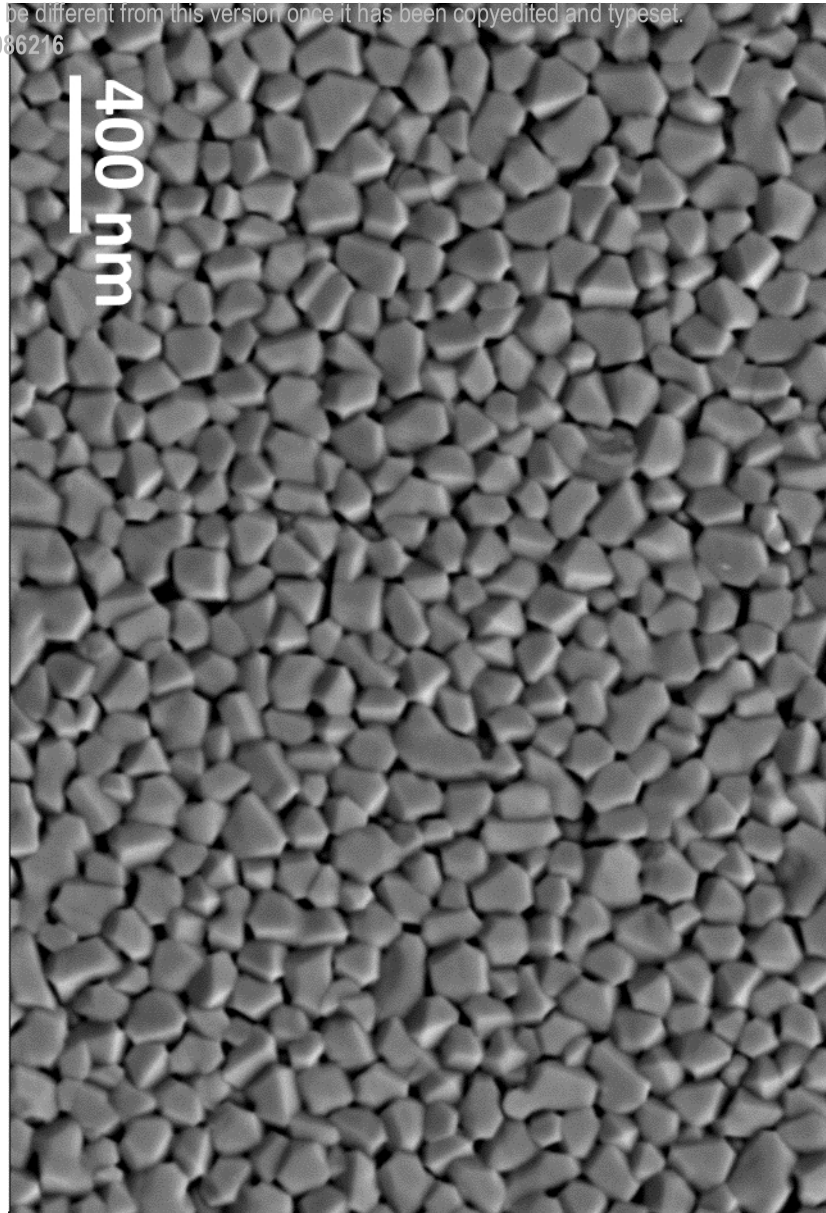

AIP Publishing

Journal of Applied Physics

ACCEPTED MANUSCRIPT

PLEASE CITE THIS ARTICLE AS DOI: 10.1063/5.0086216

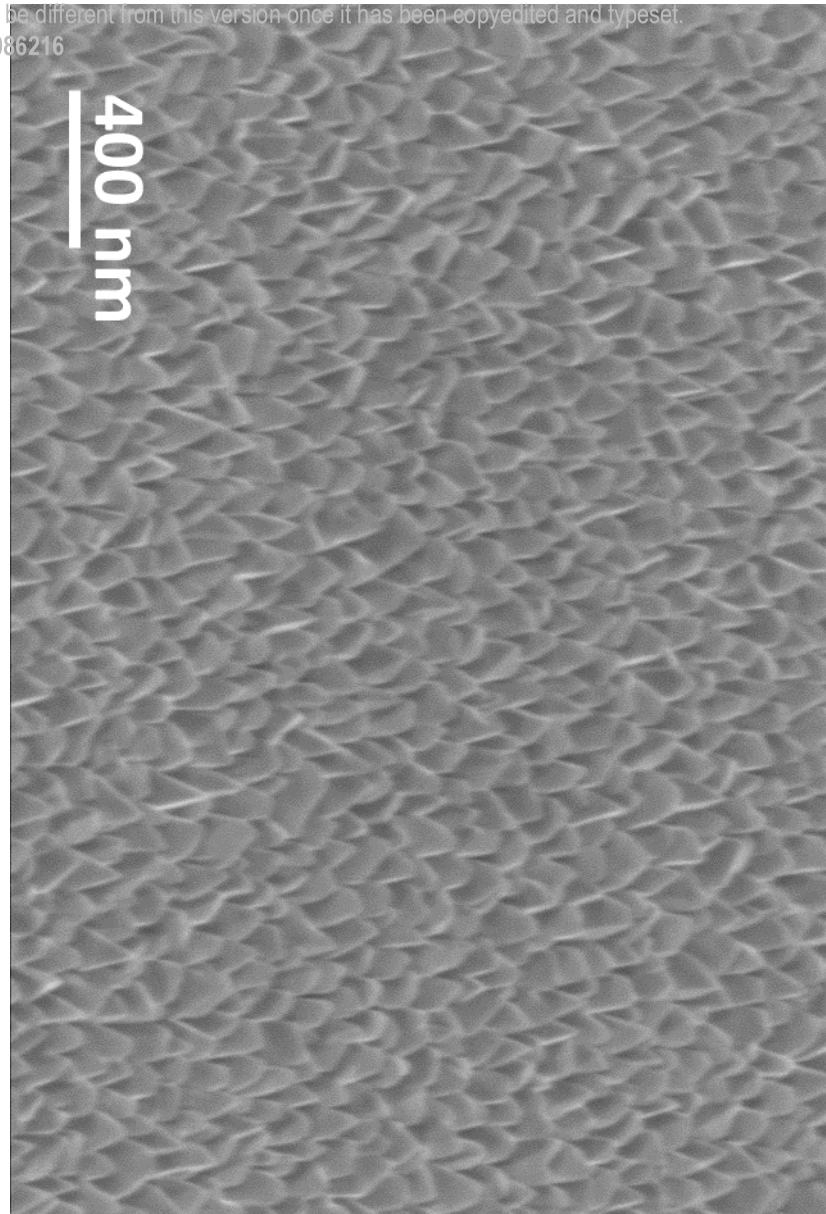

AIP Publishing

Journal of Applied Physics

ACCEPTED MANUSCRIPT

PLEASE CITE THIS ARTICLE AS DOI: 10.1063/5.0086216

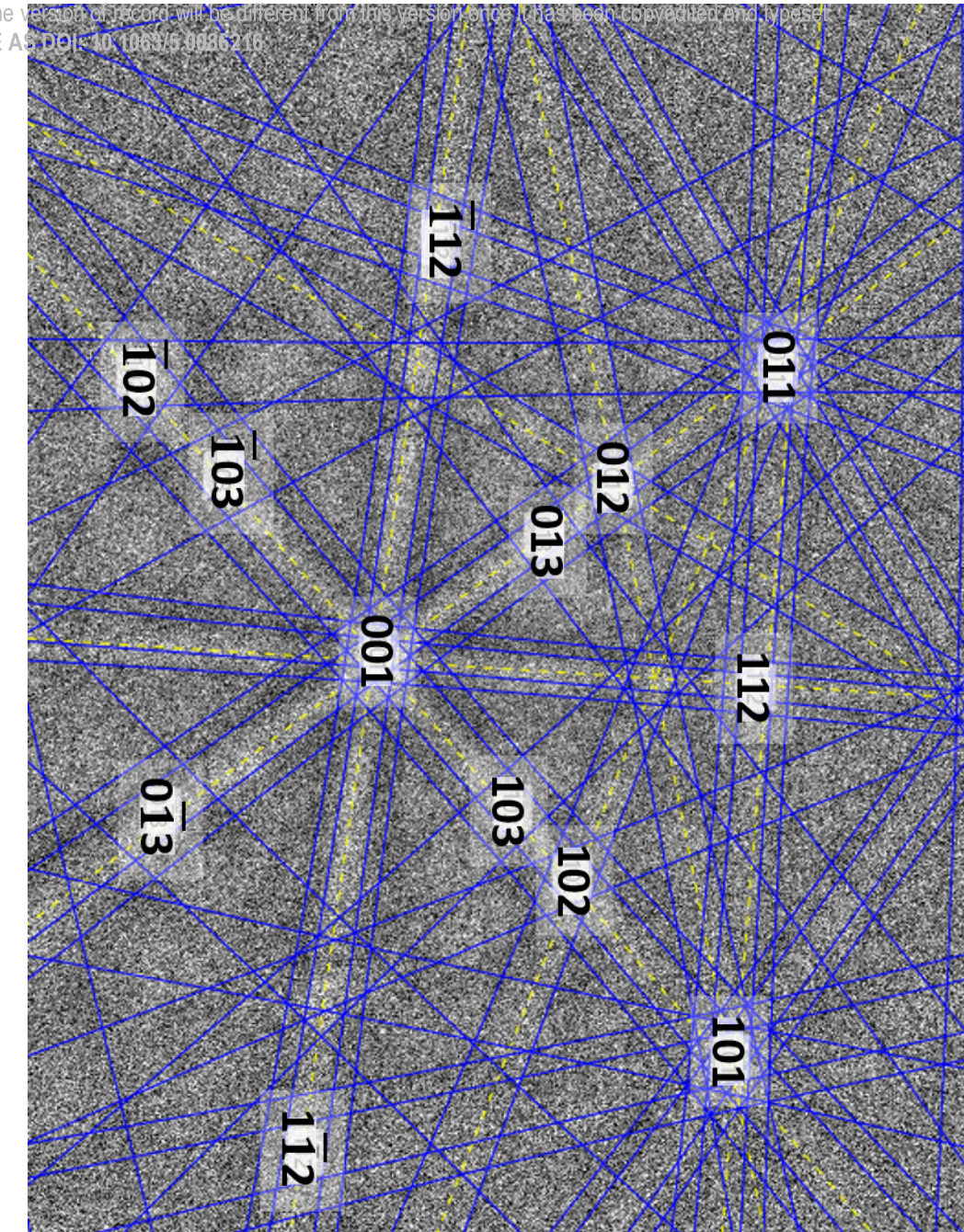

AIP Publishing

Journal of Applied Physics

ACCEPTED MANUSCRIPT

This is the author's peer reviewed, accepted manuscript. However, the online version of record will be different from this version once it has been copyedited and typeset.
PLEASE CITE THIS ARTICLE AS DOI: 10.1063/5.0086216

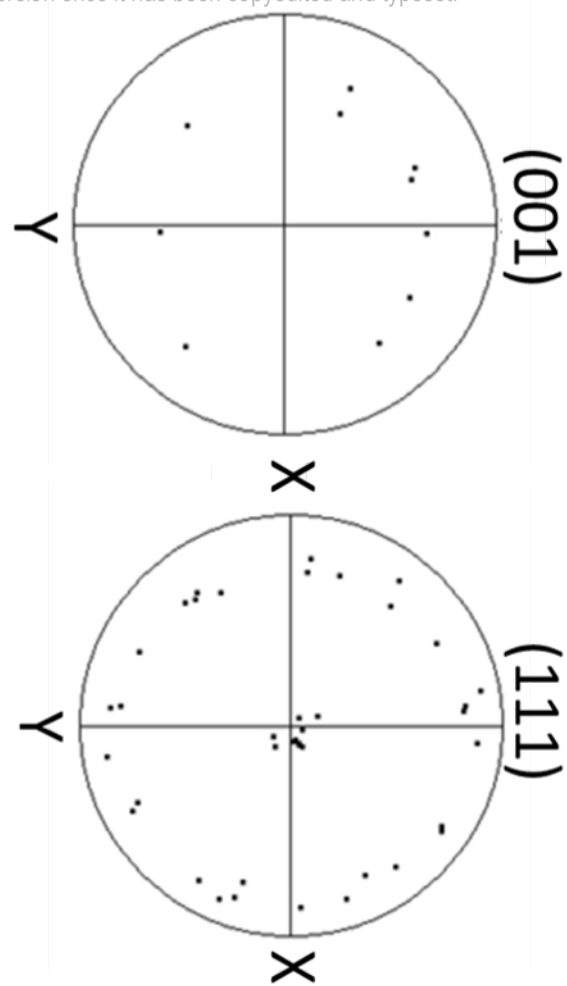

PLEASE CITE THIS ARTICLE AS DOI: 10.1063/5.0086216

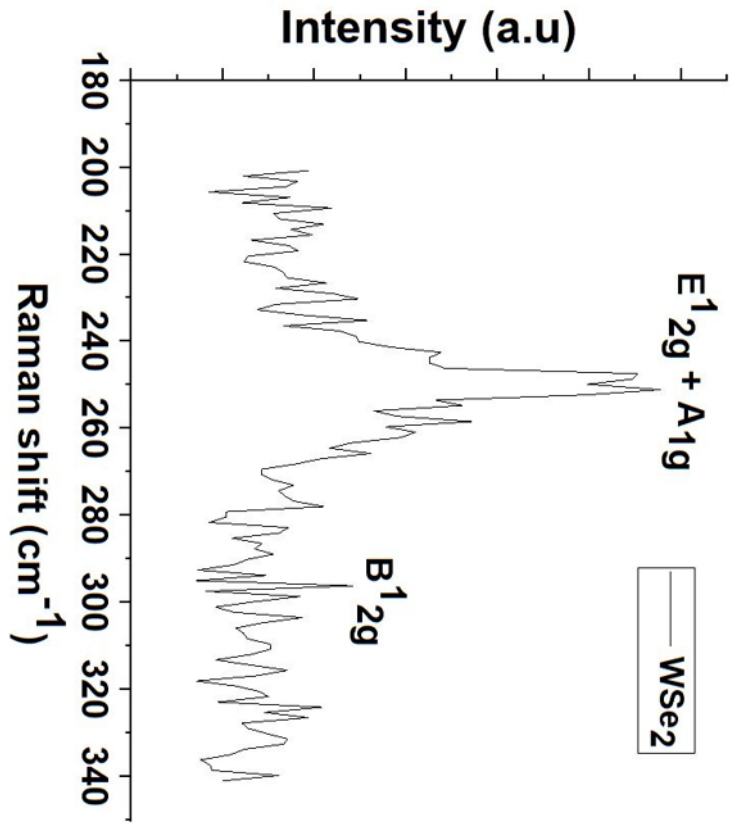

AIP Publishing

Journal of Applied Physics

ACCEPTED MANUSCRIPT

PLEASE CITE THIS ARTICLE AS DOI: 10.1063/5.0086216

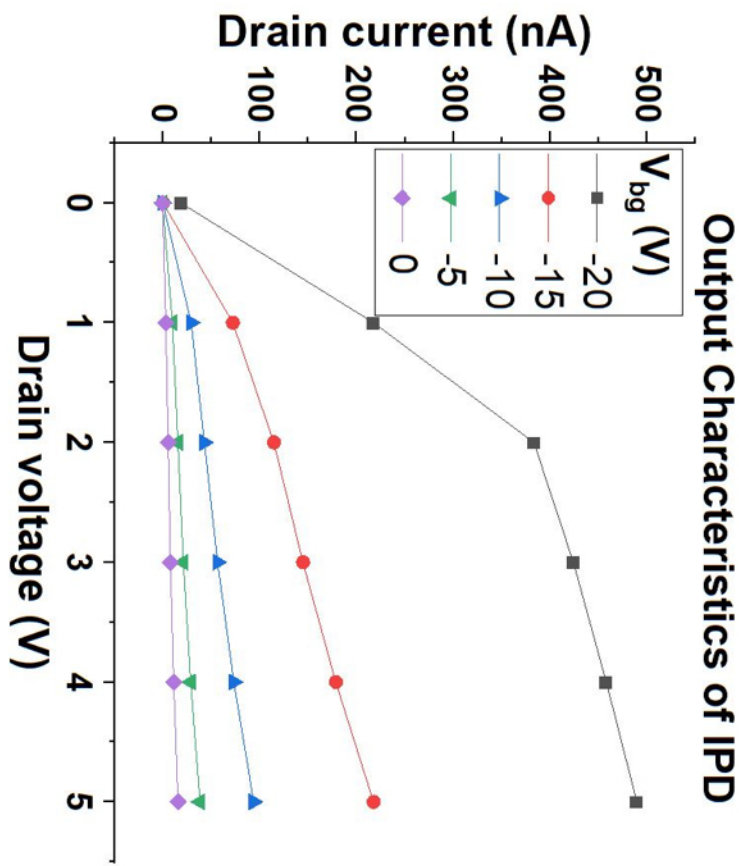

Journal of Applied Physics

AIP Publishing

AIP Publishing

Journal of Applied Physics

PLEASE CITE THIS ARTICLE AS DOI: 10.1063/5.0086216

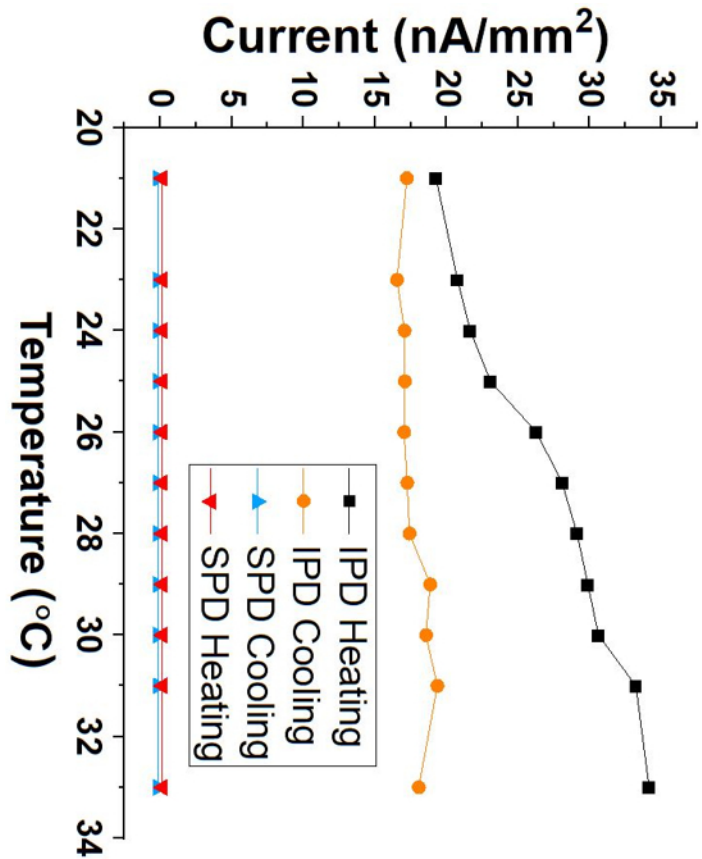

Journal of Applied Physics

PLEASE CITE THIS ARTICLE AS DOI: 10.1063/5.0086216